Available online at www.sciencedirect.com
ScienceDirect
Trans. Nonferrous Met. Soc. China 29(2019) 1728−1736
Transactions of Nonferrous Metals Society of China
www.tnmsc.cn

A new measurement method of crack propagation rate for brittle rock under THMC coupling condition

Wei YI, Qiu-hua RAO, Zhuo LI, Qing-qing SHEN
School of Civil Engineering, Central South University, Changsha 410075, China

Received 15 November 2018; accepted 30 May 2019

Abstract: A new electrical method of conductive carbon-film (with waterproof and anticorrosion ability) was proposed to continuously measure crack propagation rate of brittle rock under THMC coupling condition. A self-designed coupling testing system was used to conduct THMC coupling fracture tests of the pre-cracked red sandstone specimens (where the temperature is only changed) by this new electrical method of conductive carbon-film. Calculation results obtained by the energy method coincide well with the test results. And the higher the temperature is, the earlier the crack is initiated and the larger the crack propagation rate and accelerated velocity are, which can prove the validity of the new electrical method. This new electrical method has advantages of continuously measuring crack propagation rate over the conventional electrical, optical and acoustic methods, and can provide important basis for safety assessment and cracking-arrest design of deep rock mass engineering.

Key words: crack propagation rate; electrical method of conductive carbon-film; thermo-hydro-mechanical-chemical coupling; energy method; brittle rock

1 Introduction

The long-term effect of thermo-hydro-mechanical-chemical (THMC) coupling on rock mass in deep underground engineering (e.g., deep petroleum and mineral exploitation, geothermal energy development and nuclear waste disposal) would probably lead to initiation and propagation of the pre-existing crack and final failure of rock. Therefore, it is of great significance to study the crack propagation rate for investigation of crack propagation mechanism and design of dynamic cracking-arrest in the deep rock engineering [1−4].

Currently, test method (mechanical or physical method) is widely applied to studying crack propagation rate (v). In mechanical method, three-point bending test of double-torsion specimen was usually adopted to determine Mode I (tension) crack propagation rate of metal [5], glassy polymers [6,7] and rock [8,9] by a relationship of v and K_{I} (tensile stress intensity factor). This method has its limitation for Mode II fracture as well as Mode I fracture under THMC coupling condition. In physical methods (optical, acoustic and electric methods), high-speed digital photography was applied to measuring the crack propagation rate by photographing the specimen surface of metal [10,11], composite [12,13], and rock [14−16]. This method needs the specimen exposed outside and thus it is not suitable for tri-axial loading as well as THMC coupling condition (where the specimen is enclosed inside). Although the acoustic method can continuously monitor crack propagation rate of metal and rock under tensile [17,18], compressive [19] and complex loading condition [20,21] by the relationship between the absolute energy of acoustic emission and crack propagation rate, it is unsuitable for THMC coupling condition due to the requirement of anti-water and anti-corrosion transducer. In the electric method, the strain gauge (composed of grid metal wires at interval) is successfully used to measure the average but not real-time crack propagation rate [22−24]. For overcoming this shortage, our research group proposed a modified electric method to continuously measure the real-time crack propagation rate under TM and THM coupling loading, by using the conductive adhesive (prepared by mixing resin matrix, dispersant additive with metal powder) instead of the strain gauge at interval [25,26]. Since the conductive adhesive is water-proof but not corrosion-proof, this electric method needs

Foundation item: Projects (51474251, 51874351) supported by the National Natural Science Foundation of China
Corresponding author: Qiu-hua RAO; Tel: +86-731-88876841; E-mail: raoqh@csu.edu.cn
DOI: 10.1016/S1003-6326(19)65080-6

to be further developed.

In this work, a new electrical method was proposed to continuously measure the crack propagation rate of brittle rock under THMC coupling condition, in which the conductive carbon-film replaced the conductive adhesive. A calculation formula of THMC coupling crack propagation rate was deduced by the energy method in order to verify the validity of the new electrical method. Research results would provide an important basis for fracture mechanism investigation, crack-arrest design and disaster prevention for brittle rock under THMC coupling condition.

2 Conductive carbon-film electrical method

2.1 Conductive carbon-film

Conductive carbon-film (0.2 mm in thickness) consists of carbon powders with good conductivity (dielectric constant k=50 Ω/mm) and paper pulp. It can resist both water and chemical corrosion and has better heat stability and more stable electric resistance than the conductive adhesive (painted on the specimen surface) [26]. Therefore, it can act as a strain gauge to continuously monitor the crack propagation rate of brittle rock under THMC coupling condition.

Before the test, the conductive carbon-film must be glued tightly and uniformly on the smooth specimen surface near the crack tip along its predicted propagation direction by fracture criterion. As shown in Fig. 1, part of the pre-crack length ($0.5a_0 \le l_0 \le a_0$, $w=l_0$, a_0 is initial crack length, and w is glued width of conductive carbon-film) is covered in order to prevent too small resistance at the crack initiation from influencing testing precise. In this case, the conductive carbon-film glued on the pre-cracked specimen becomes a variable resistance (R) related to crack propagation length (l), where two leading wire points of A (positive pole) and B (negative pole) are located symmetrically with the original crack plane for measuring its resistance:

$$R=2k(l_0+l) \tag{1}$$

2.2 Electric circuit

Figure 2 shows a circuit diagram of conductive carbon-film electrical method, where R_0 is a series resistance (R_0=500 Ω) and U_0 is the power voltage (U_0=20 V). When the crack initiates to propagate at a length of l, the conductive carbon-film glued on the pre-cracked specimen surface would tear open and the electric current moves along the direction of its smallest resistance, i.e., $A \to C \to B$, regardless of the small crack width (Fig. 1).

The voltage of the conductive carbon-film (U) is

$$U=\frac{U_0 R}{R_0+R} \tag{2}$$

Substituting Eq. (1) into Eq. (2) leads to

$$l=\frac{1}{2k}\left(\frac{UR_0}{U_0-U}-2kl_0\right) \tag{3}$$

Therefore, the crack propagation rate can be obtained by the tested $U-t$ (time) curve:

$$v=\frac{\mathrm{d}l}{\mathrm{d}t}=\frac{R_0}{k}\left[\frac{U_0}{(U_0-U)^2}\cdot\frac{\mathrm{d}U}{\mathrm{d}t}\right] \tag{4}$$

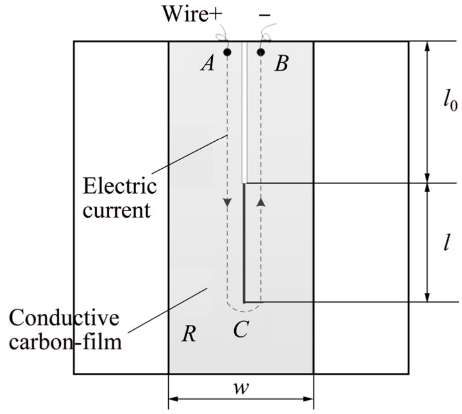

Fig. 1 Schematic diagram of conductive carbon-film glued on pre-cracking specimen

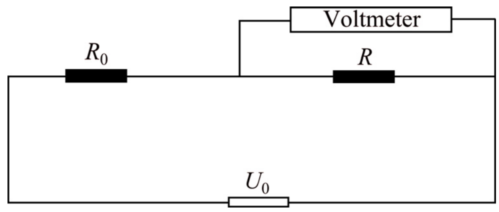

Fig. 2 Circuit diagram of conductive carbon-film electrical method

3 Measurement of THMC coupling crack propagation rate

3.1 Rock specimen

Red sandstone exploited from Yunnan province in China was adopted in the test. It has main mineral composition of 69.1% quartz, 13.4% feldspar, 6.2% calcite and 3.6% dolomite (determined by X-ray diffraction test). Figure 3 shows a well-prepared standard cylinder specimen of red sandstone (d50 mm × 100 mm) with an inclined penetrating crack (β=45°, $2a$=30 mm, h=2 mm). An additional vertical hole (d3 mm × 50 mm) is drilled from the bottom center of the specimen to the original crack surface for applying the hydraulic pressure σ_{H} onto the original crack surface.

Considering that this study is focused on a new measurement method of the crack propagation rate, a specific THMC coupling condition was selected for red sandstone tests, in which the temperature is only changed while the others are unchanged (Table 1). Since the chemical solution would cause corrosion of tri-axial chamber loading setup, the chemical effect is applied by the soaking test, i.e., the red sandstone specimen was soaked in the chemical solution (pH=2) for 120 h at a specific temperature until the chemical solution (pH value) was not changed any more. After the soaking test, its main mechanical parameters at room and high temperatures were obtained by ISRM (International Society of Rock Mechanics) suggested testing methods [27], including tensile strength (σ_t), uni-axial compressive strength (σ_c), elastic modulus (E), Poisson ratio (v), cohesion (c), internal friction angle (φ), Mode I (tension) and Mode II (shear) fracture toughness (K_{IC} and K_{IIC}), and Mode I and Mode II fracture energy release rate (G_{IC} and G_{IIC}) (Table 2 and Table 3).

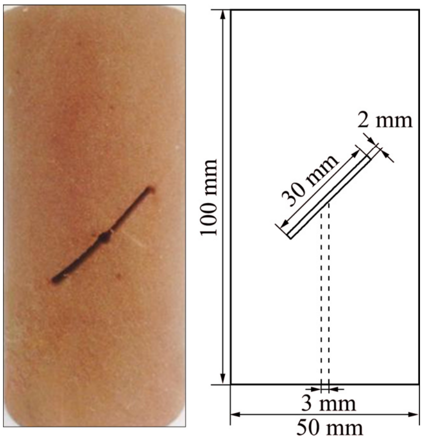

Fig. 3 Red sandstone cylinder specimen with an inclined penetrating crack

Table 1 THMC coupling conditions

No.	T/°C	σ_H/MPa	σ_M/MPa	pH
T1	20	4	6	2
T2	50	4	6	2
T3	90	4	6	2

Table 2 Main mechanical parameters of red sandstone at room temperature

σ_t/MPa	σ_c/MPa	E/GPa	v	c/MPa	φ/(°)
6.12	56.1	11.21	0.29	13.7	32

3.2 Location of conductive carbon-film

For determining the location of conductive carbon-film glued on the rock specimen, it is necessary to predict its crack propagation trajectories by fracture criterion firstly. Currently, there exist mainly three types of fracture criteria: (1) stress-based fracture criterion [28−30], (2) strain-based fracture criterion [31] and (3) energy-based fracture criterion [32−34]. These fracture criteria can predict Mode I (tensile) fracture under pure tensile, pure shear and mixed-mode loading, but not the true Mode II (shear) fracture (caused by maximum shear stress). A new fracture criterion of maximum tensile and shear stress intensity factor ratio proposed by our research group can successfully predict Mode I or Mode II fracture under mixed-mode loading conditions [35] as well as under multiple-field coupling condition [36,37].

Table 3 Elastic modulus and fracture parameters at different temperatures

No.	T/°C	E/GPa	K_{IC}/(MPa·m$^{0.5}$)
T1	20	11.21	0.92
T2	50	10.96	0.79
T3	90	10.23	0.58

No.	K_{IIC}/(MPa·m$^{0.5}$)	$G_{IC}(=K_{IC}^2/E)$/(N·m^{-1})	$G_{IIC}(=K_{IC}^2/E)$/(N·m^{-1})
T1	1.57	75.5	219.9
T2	1.39	56.9	176.3
T3	0.93	32.9	84.5

For the pre-cracked rock specimen (Fig. 4), the crack-tip tensile and shear stress intensity factors along an arbitrary direction (α) are

$$\begin{cases} K_I(\alpha)=K_I\cos^3\dfrac{\alpha}{2}-3K_{II}\sin\dfrac{\alpha}{2}\cos^2\dfrac{\alpha}{2} \\ K_{II}(\alpha)=K_I\sin\dfrac{\alpha}{2}\cos^2\dfrac{\alpha}{2}+ \\ \quad K_{II}\cos\dfrac{\alpha}{2}(1-3\sin^2\dfrac{\alpha}{2}) \end{cases} \tag{5}$$

where K_I and K_{II} are the crack-tip tensile and shear stress intensity factors on its original plane, respectively.

K_I and K_{II} become

$$\begin{cases} K_I=[\dfrac{(\sigma_L+\sigma_M)}{2}+\dfrac{(\sigma_L-\sigma_M)}{2}\cos 2\theta+\sigma_H]\sqrt{\pi a} \\ K_{II}=[\dfrac{(\sigma_L-\sigma_M)}{2}\cos 2\theta]\sqrt{\pi a} \end{cases} \tag{6}$$

where tensile stress is defined to be positive.

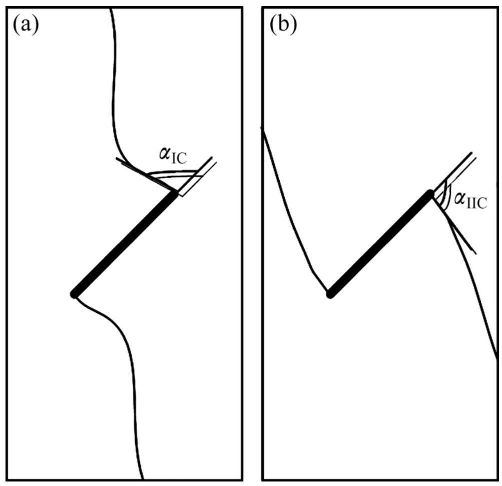

Fig. 4 Fracture mode of pre-cracked rock specimens: (a) Mode I fracture (α_{IC}>0); (b) Mode II fracture (α_{IIC}<0)

According to this new criterion [35], Mode I fracture occurs when the ratio of maximum crack-tip shear to tensile stress intensity factor is smaller than the ratio of Mode II to Mode I fracture toughness of the material and the maximum tensile stress intensity factor reaches its Mode I fracture toughness. Otherwise, Mode II fracture occurs. Therefore, Mode I or Mode II crack initiation angles (α_{IC} or α_{IIC}) and loads (σ_{LIC} or σ_{LIIC}) under different THMC coupling conditions can be determined as follows:

$$\begin{cases} \dfrac{K_{II}(\alpha)_{max}}{K_I(\alpha)_{max}} < \dfrac{K_{IIC}}{K_{IC}} \\ K_I(\alpha)_{max} = K_{IC} \end{cases} \Rightarrow \begin{cases} \alpha_{IC} \\ \sigma_{LIC} \end{cases}, \text{ Mode I fracture}$$

or

$$\begin{cases} \dfrac{K_{II}(\alpha)_{max}}{K_I(\alpha)_{max}} > \dfrac{K_{IIC}}{K_{IC}} \\ K_{II}(\alpha)_{max} = K_{IIC} \end{cases} \Rightarrow \begin{cases} \alpha_{IIC} \\ \sigma_{LIIC} \end{cases}, \text{ Mode II fracture} \tag{7}$$

Table 4 lists the calculation values of crack initiation angles and loads under different THMC coupling conditions by substituting three groups of parameters into the new criterion: (1) crack length $2a$ and inclination angle θ, (2) THMC loading condition (T, P_H, P_M, pH) and (3) fracture toughness (K_{IC} and K_{IIC}). When the temperature is increased, the fracture mode is changed from Mode II (α_{IIC}<0) to Mode I (α_{IC}>0) since the higher the temperature is, the larger the ratio of K_{IIC}/K_{IC} is (Table 3) and thus the more difficultly the Mode II fracture occurs. The conductive carbon-film needs to be glued exactly and tightly along the predicted crack propagation trajectory for measuring its propagation rate (Fig. 5).

Table 4 Crack initiation angle under different THMC coupling conditions

No.	T/°C	σ_{LIC} (or σ_{LIIC})/ MPa	α_{IC} (or α_{IIC})/ (°)	Fracture mode
T1	20	21.7	−108.1	Mode II
T2	50	20.1	−108.9	Mode II
T3	90	15.1	98.7	Mode I

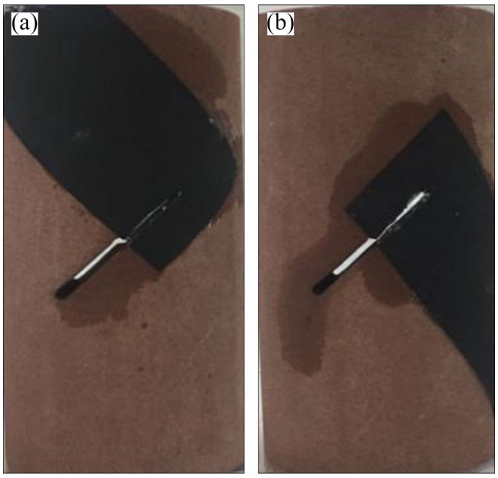

Fig. 5 Location of conductive carbon-film glued on pre-cracked rock specimen: (a) Mode I fracture; (b) Mode II fracture

3.3 Testing system and procedure

Figure 6 shows a self-designed coupling testing system, including axial pressure loading system, hydraulic pressure and confining pressure loading system. The water and oil were heated to the specific temperature (T) and then injected into the hydraulic pressure system (σ_H) and tri-axial chamber (σ_M), respectively. Let

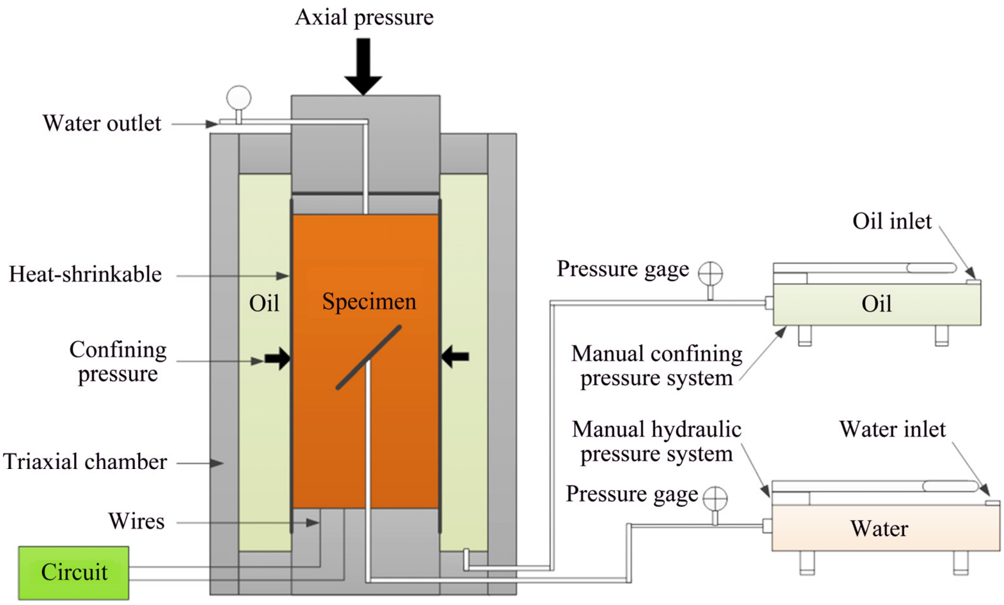

Fig. 6 Self-designed coupling testing system

T<100 °C for preventing the evaporation of water and σ_H<σ_M for avoiding the mixture of the water and oil.

Considering that chemical solution (pH=2) would have corrosion influence on tri-axial chamber loading setup and water pipe, the rock specimens were first soaked in chemical solution (pH=2) at different temperatures and then dried and rapidly glued with the conductive carbon-film along its predicted crack propagation trajectory. After being tightly wrapped by a heat-shrinkable hose of high-strength, it is finally put into the tri-axial chamber and loaded at a constant rate of 0.1 mm/min until failure.

3.4 Test result and analysis

Figure 7 shows fracture trajectories of red sandstone specimens at different temperatures under THMC coupling condition. The fracture mode is changed from Mode II to Mode I when the temperature is increased, which coincides well with that by the new criterion.

Figures 8 and 9 show the voltage−time (U−t) and axial stress−time (σ_L−t) curves of the red sandstone specimen under different THMC coupling conditions, respectively, where σini L and t_i are initiation stress and time, respectively, and σ_L^{un} and t_u are unstable propagation stress (tensile strength) and time, respectively. The crack propagation length−time (l−t) and crack propagation rate−time (v−t) curves can be obtained by Eqs. (3) and (4), respectively, as shown in Figs. 9 and 10.

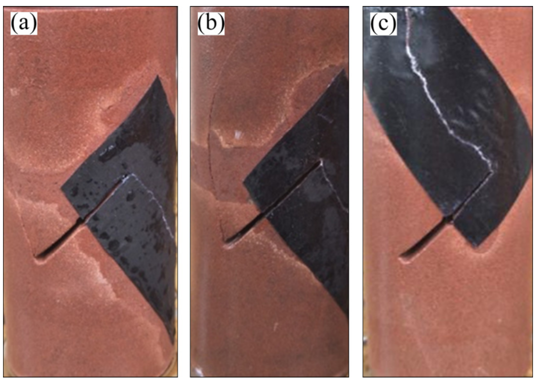

Fig. 7 Fracture trajectories of red sandstone specimen at different temperatures (σ_H=4 MPa, σ_M=6 MPa, pH=2): (a) T1 (20 °C); (b) T2 (50 °C); (c) T3 (90 °C)

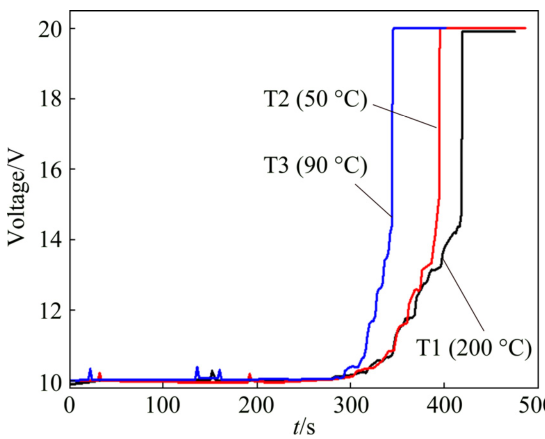

Fig. 8 Voltage−time curves of conductive carbon-film at different temperatures

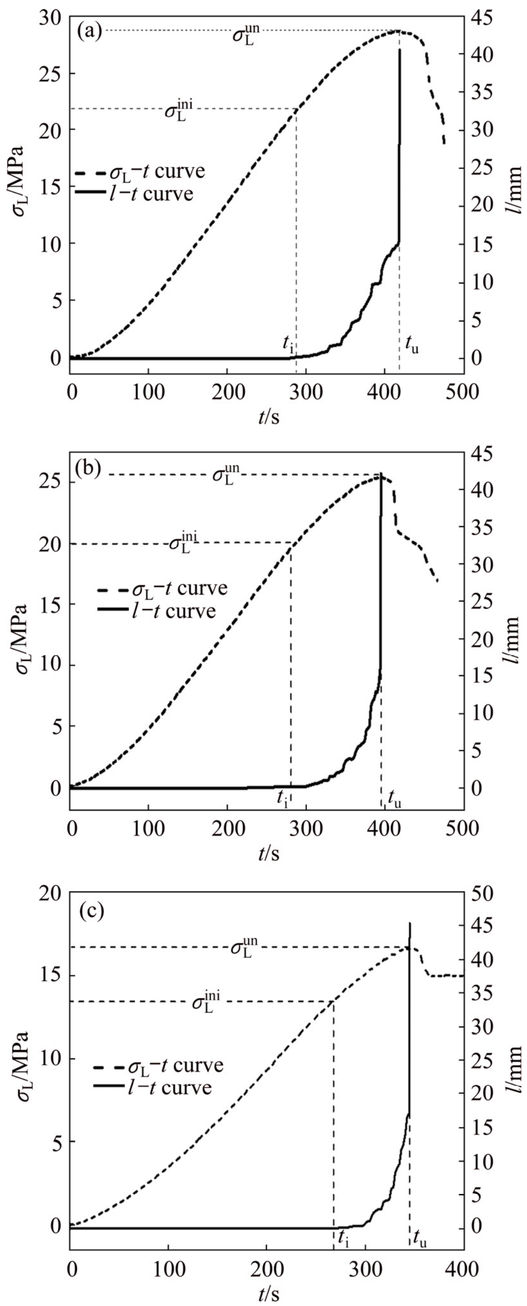

Fig. 9 Curves of axial stress and crack propagation length varying with time at different temperatures (σ_H=4 MPa, σ_M=6 MPa, pH=2): (a) T1 (T=20 °C); (b) T2 (T=50 °C); (c) T3 (T=90 °C)

All of l−t curves are divided into three parts: horizontal line (no crack propagation when $\sigma_L<\sigma_L^{ini}$), slope-increased curve (crack stable propagation when $\sigma_L^{ini}<\sigma_L<\sigma_L^{un}$), and vertical line (crack unstable propagation when $\sigma_L=\sigma_L^{un}$). The higher the temperature is, the earlier the crack initiates to propagate. This is because high temperature would result in decrease of fracture toughness (Table 3) and promote the crack initiation.

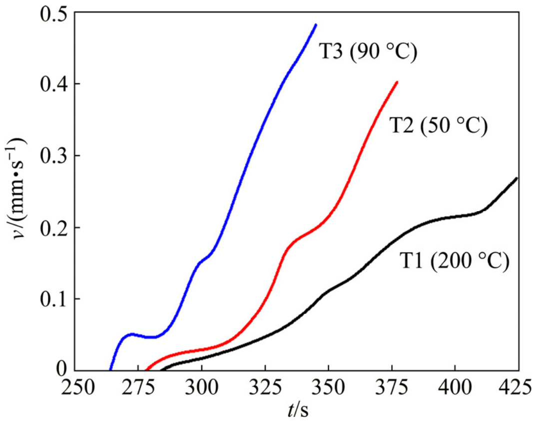

Fig. 10 Crack propagation rate at different temperatures

The v−t curves at different temperatures increase in fluctuation in the early stage of crack initiation and then tend to increase stably. This is because the original crack initiation is accompanied with the occurrence of micro-cracks at crack tip (inside the red sandstone specimen), which consumes a part of energy (used to promote the original crack propagation). Furthermore, the higher the temperature is, the shorter the time of v−t curves in fluctuation is, since high temperature accelerates the occurrence of micro-cracks at crack tip in a short time. The crack propagation rate and accelerated velocity are increased with an increase in temperature. This is due to the fact that red sandstone is mainly composed of crystal and clay cement, and high temperature promotes the chemical reaction velocity of clay cement and decreases its mechanical properties.

4 Verification of THMC coupling crack propagation rate

4.1 Formula derivation

Figure 11 shows calculation model of the same pre-cracked cylinder specimen as the tested specimen under THMC coupling condition. According to energy method, total THMC loading work (W_{THMC}) consists of the heat energy (W_T), hydraulic pressure work (W_H), confining pressure work (W_M), axial pressure work (W_L), and chemical reaction heat energy (W_C):

$$W_{THMC}=W_T+W_H+W_M+W_L+W_C$$
$$=\int\alpha_T E\mathrm{d}T+\int P_H\mathrm{d}l_H+\int P_M\mathrm{d}l_M+\int\mathrm{d}P_L l_L+W_C \quad (8)$$

where α_T is thermal expansion coefficient of rock, and l_H, l_M and l_L are the crack surface, circumferential and axial displacements, respectively.

Figure 12 shows the schematic diagram of stress−strain curve. It consists of four stages: (1) non-linear compaction (OA), (2) elastic deformation (AB), (3) non-elastic deformation (BC) and (4) failure (CD), where σ_L^{ini} and ε_i are the crack initiation stress and strain, respectively, and σ_L^{un} and ε_u are the crack unstable propagation stress (compressive strength) and strain, respectively.

When the crack initiates to stably propagate ($\sigma_L^{ini}<\sigma_L<\sigma_L^{un}$), total energy at any point J can be expressed by the enclosed area of $OABJFO$, including the dissipation energy of non-linear compaction (U_{d1}), non-elastic deformation (U_{d2}), and elastic strain energy (U_e). In Fig. 12, JH is unloading straight line ($JH//BI$). U_{d1} is almost unchanged for the same rock material under a specific THMC loading condition and U_{d2} is the sum of fracture surface energy ($\Gamma=2G_CA$, where G C is fracture

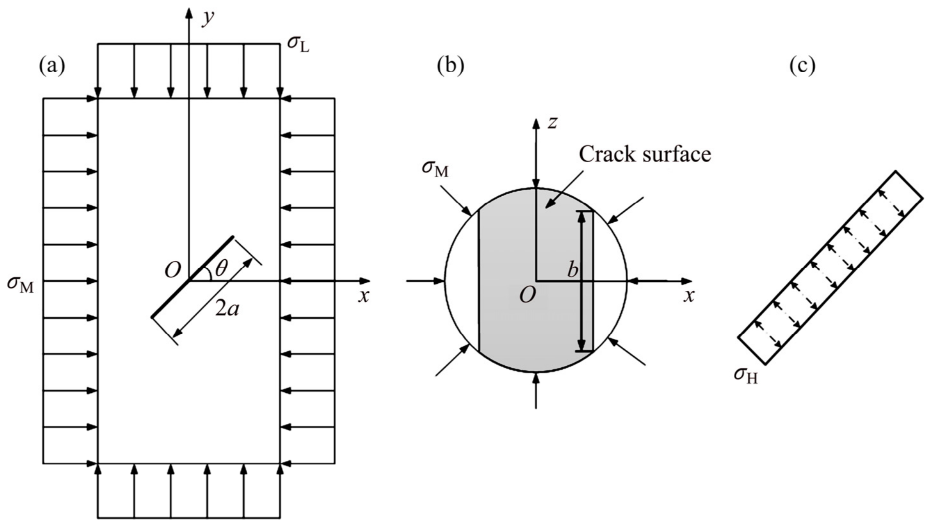

Fig. 11 Pre-cracked cylinder specimen model under THMC coupling condition: (a) Front view; (b) Projection of crack plane on cross-section plane; (c) Enlarged crack surface

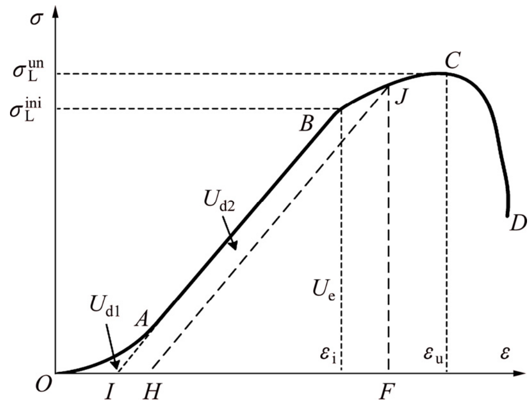

Fig. 12 Schematic diagram of stress−strain curve

energy release rate and A is crack propagation area) and plastic-deformation dissipation energy (U_p):

$$U_J = U_{d1} + U_{d2} + U_e = U_{d1} + 2G_C A + U_p + U_e \quad (9)$$

$$U_e = \int \frac{1}{2E}[\sigma_L^2 + 2\sigma_M^2 - 2\nu(2\sigma_L\sigma_M + \sigma_M^2)]dV \quad (10)$$

According the energy method, THMC loading work (W_{THMC}) is exchanged into energy of the point J, i.e.,

$$W_{THMC} = U_{d1} + 2G_C A + U_p + U_e + U_k \quad (11)$$

Substituting Eq. (8) into Eq. (11) becomes

$$\int \alpha_T E dT + \int dP_L l_L + \int P_H dl_H + \int P_M dl_M + W_C$$
$$= U_{d1} + 2G_C A + U_p + U_e + U_k \quad (12)$$

Since THMC coupling fracture test was conducted at a specific temperature after the soaking test of red sandstone specimen, the temperature (T) and chemical reaction heat energy (W_C) keep constant. Taking the derivation of Eq. (12) with respect to time (t) leads to

$$\frac{dP_L l_L}{dt} + \frac{P_H dl_H}{dt} + \frac{P_M dl_M}{dt} = \frac{dU_e}{dt} + \frac{2G_C dA}{dt} + \frac{dU_p}{dt} + \frac{dU_k}{dt} \quad (13)$$

where

$$dA = 2b dl \quad (14)$$

where b is projection width of the crack surface on xOz plane related to l (Fig. 11(b)).

Assuming that the original crack is stably extended in the straight line, there is

$$b = 2\sqrt{r^2 - [a\cos\theta + l\cos(\theta + \alpha)]^2} \quad (15)$$

where α is the crack initiation angle, r is the radius of the cylinder (r=25 mm). When l=0 (without crack initiation), b=45.28 mm (initial crack width).

Since the red sandstone is brittle material, its plastic deformation could be disregarded ($U_p \approx 0$). When the crack propagates at a relatively small rate, its kinetic energy (U_k) could be neglected ($U_k \approx 0$). Substituting Eq. (14) into Eq. (13) yields

$$v_t = \left(\frac{P_L dl_L}{dt} + \frac{l_L dP_L}{dt} + \frac{P_H dl_H}{dt} + \frac{P_M dl_M}{dt} - \frac{dU_e}{dt}\right) / 2G_C b \quad (16)$$

Obviously, the crack propagation rate would be increased with decrease of the fracture energy release rate (G_C) caused by increase of the temperature.

4.2 Calculation result and analysis

The crack propagation rate v_t can be calculated by the test result of P_L, l_L, l_H, l_M and U_e as follows: (1) P_L−t relation expression is determined by the polynomial fitting method based on the axial stress−time curve; (2) dl_L/dt=1.67×10^{-3} mm/s (the loading rate is 0.1 mm/min); (3) The hydraulic pressure work ($P_H dl_H$) could be ignored since P_H does a positive and negative work on the upper and lower crack surface simultaneously (assuming $l_{H+} \approx l_{H-}$); (4) l_M−t relation is approximately expressed by Poisson ratio and l_L regardless of plastic deformation (i.e., $dl_M/dt \approx -0.48\times10^{-3}$ mm/s); (5) U_e−t relation can be calculated by substituting the axial pressure and the confining pressure into Eq. (10). Table 5 gives these polynomial fitting results of P_L−t and U_e−t with good regression coefficients of R^2=0.999 and 0.999.

Table 5 Polynomial fitting results (Specimen T1)

Curve	Polynomial fitting expression	R^2
P_L−t	$P_L(t)=-0.63+3.7\times10^{-2}t+7.85\times10^{-4}t^2-9.82\times10^{-7}t^3-1.96\times10^{-10}t^4$	0.999
U_e−t	$U_e(t)=4.67\times10^{-7}-1.26\times10^{-9}t-2.34\times10^{-11}t^2+1.65\times10^{-13}t^3+1.24\times10^{-15}t^4-3.53\times10^{-18}t^5+1.49\times10^{-21}t^6+8.74\times10^{-25}t^7+8.74\times10^{-29}t^8$	0.999

Therefore, the calculation results of v_t−t curves under different THMC loading conditions can be obtained by substituting the polynomial fitting expression of the test result into Eq. (16), as shown in Fig. 13. It is seen that the crack propagation rate and accelerated velocity in calculation results have the same rule as those in test results, i.e., the higher the temperature is, the larger the crack propagation rate and accelerated velocity are. There exists a small error between the test and calculation results of v_t−t. This is because the neglect of the plastic-deformation dissipation energy and crack-propagation kinetic energy would lead to calculation results larger than test results.

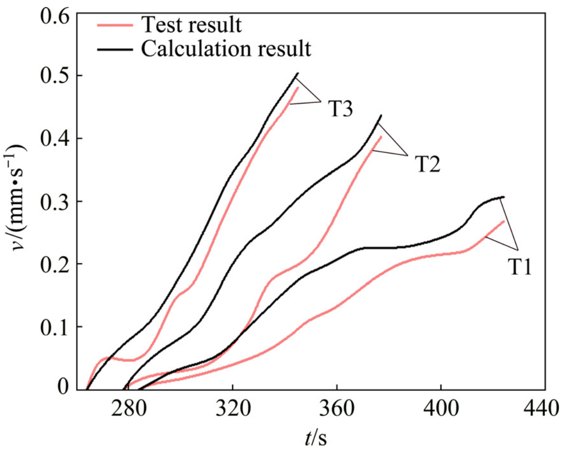

Fig. 13 Calculation results of crack propagation rate at different temperatures

5 Conclusions

(1) A new electrical method of conductive carbon-film (with waterproof and anticorrosion ability) is proposed to continuously measure the crack propagation rate of brittle rock under THMC coupling condition successfully. It can overcome the shortages of the conventional electrical method (which is inapplicable for continuous measurement of crack propagation rate because of the strain gauges at interval), the optical method and acoustic methods (which are unsuitable for multiple-field coupling loading condition).

(2) For ensuring the measurement precision, the conductive carbon-film must be firstly located along the predicted crack propagation trajectory and covering part of the initial crack length ($0.5a_0-a_0$) and then glued tightly and uniformly on the smooth specimen surface.

(3) The measured THMC coupling crack propagation rate is increased as the axial stress is increased. The higher the temperature is, the earlier the crack initiates to propagate and the larger the crack propagation rate and accelerated velocity are.

(4) A calculation formula of THMC coupling crack propagation rate is deduced based on the energy method. The calculated crack propagation rate and accelerated velocity are increased with an increase in temperature and they are in good agreement with the test results, which could prove the validity of the newly proposed conductive carbon-film electric method.

References

[1] YUI M. A research program for numerical experiments on coupled thermo-hydro-mechanical and chemical processes [J]. Nature, 2002, 300(5894): 747−750.

[2] TSANG C F. Introductory editorial to the special issue on the DECOVALEX-THMC project [J]. Environmental Geology, 2009, 57(6): 1217−1219.

[3] ZHENG L, RUTQVIST J, XU H, BIRKHOLZER J T. Coupled THMC models for bentonite in an argillite repository for nuclear waste: Illitization and its effect on swelling stress under high temperature [J]. Engineering Geology, 2017, 230: 118−129.

[4] KAMALI-ASL A, GHAZANFARI E, PERDRIAL N, BREDICE N. Experimental study of fracture response in granite specimens subjected to hydrothermal conditions relevant for enhanced geothermal systems [J]. Geothermics, 2018, 72: 205−224.

[5] JAHEDI M, PAYDAR M H, KNEZEVIC M. Enhanced microstructural homogeneity in metal-matrix composites developed under high-pressure-double-torsion [J]. Material Characterization, 2015, 104: 92−100.

[6] SHINDO Y, NARITA F, MIKAMI M. Double torsion testing and finite element analysis for determining the electric fracture properties of piezoelectric ceramics [J]. Journal of Applied Physics, 2005, 97(11): 109−114.

[7] BECKER T H, MARROW T J, TAIT R B. An evaluation of the double torsion technique [J]. Experimental Mechanics, 2011, 51(9): 1511−1526.

[8] YUAN Hai-ping, CAO Ping, XU Wan-zhong. Mechanism study on subcritical crack growth of flabby and intricate ore rock [J]. Transactions of Nonferrous Metals Society of China, 2006, 16(3): 723−727.

[9] NARA Y, YAMANAKA H, OE Y, KANEKO K. Influence of temperature and water on subcritical crack growth parameters and long-term strength for igneous rocks [J]. Geophysical Journal International, 2018, 191(2): 47−60.

[10] SHI X, EVANS B L, FLYNN D I, CAO E. The study of island growth of ion beam sputtered metal films by digital image processing [J]. Thin Solid Films, 1994, 238(1): 54−61.

[11] PERALTA P, CHOI S H, GEE J. Experimental quantification of the plastic blunting process for stage II fatigue crack growth in one-phase metallic materials [J]. International Journal of Plasticity, 2007, 23(10): 1763−1795.

[12] AVACHAT S, ZHOU M. High-speed digital imaging and computational modeling of dynamic failure in composite structures subjected to underwater impulsive loads [J]. International Journal of Impact Engineering, 2015, 77: 147−165.

[13] HOU F, HONG S. Characterization of R-curve behavior of translaminar crack growth in cross-ply composite laminates using digital image correlation [J]. Engineering Fracture Mechanics, 2014, 117(1): 51−70.

[14] LE J L, MANNING J, LABUZ J F. Scaling of fatigue crack growth in rock [J]. International Journal of Rock Mechanics and Mining Sciences, 2014, 72(72): 71−79.

[15] GAO G, HUANG S, XIA K, LI Z. Application of digital image correlation (DIC) in dynamic notched semi-circular bend (NSCB) tests [J]. Experimental Mechanics, 2015, 55(1): 95−104.

[16] XING H Z, ZHANG Q B, BRAITHWAITE C H, PAN B, ZHAO J. High-speed photography and digital optical measurement techniques for geomaterials: Fundamentals and applications [J]. Rock Mechanics and Rock Engineering, 2017, 50: 1−49.

[17] HOLLMANN K, HAHN H T. Acoustic emission behavior of epoxies during tensile loading [J]. Polymer Engineering and Science, 1989, 29(8): 513−522.

[18] SINGH S K, SRINIVASAN K, CHAKRABORTY D. Acoustic emission studies on metallic specimen under tensile loading [J]. Material Design, 2003, 24(6): 471−481.

[19] HARRIS D O, DUNEGAN H L. Continuous monitoring of fatigue-crack growth by acoustic-emission techniques [J]. Experimental Mechanics, 1974, 14(2): 71−81.

[20] WU Jin-wen. Experimental study of acoustic emission of granite due to thermal cracking under high temperature and isostatic stress [J]. Journal of China Coal Society, 2012, 37(7): 1111−1117. (in Chinese)

[21] KONSZTOWICZ K J. Crack growth and acoustic emission in ceramics during thermal shock [J]. Journal of the American Ceramic Society, 2010, 73(3): 502−508.
[22] DAI F, XIA K, ZHENG H, WANG Y X. Determination of dynamic rock Mode-I fracture parameters using cracked chevron notched semi-circular bend specimen [J]. Engineering Fracture Mechanics, 2011, 78(15): 2633−2644.
[23] ZHANG Q B, ZHAO J. Effect of loading rate on fracture toughness and failure micromechanisms in marble [J]. Engineering Fracture Mechanics, 2013, 102(2): 288−309.
[24] YANG Jing-rui, ZHANG Cai-gui, ZHOU Yan, ZHU Zhe-ming, WANG Qi-zhi. A new method for determining dynamic fracture toughness of rock using SCDC specimens [J]. Chinese Journal of Rock Mechanics and Engineering, 2015, 34(2): 279−292. (in Chinese)
[25] RAO Qiu-hua, XIE Hai-feng, XIE Qiang. In-plane shear (Mode II) crack sub-critical propagation of rock at high temperature [J]. Journal of Central South University, 2008, 15(S1): s402−s405.
[26] LI Zhuo, RAO Qiu-hua, LI Peng, YI Wei. Crack initiation rate of brittle rock under thermal-hydro-mechanical coupling condition [J]. Transactions of Nonferrous Metals Society of China, 2018, 28(10): 2107−2113.
[27] FAIRHURST C E, HUDSON J A. Draft ISRM suggested method for the complete stress-strain curve for intact rock in uniaxial compression [J]. International Journal of Rock Mechanics and Mining Sciences, 1999, 36(3): 281−289.
[28] ERDOGAN F, SIH G C. On the crack extension in plates under plane loading and transverse shear [J]. Basic Engineering, 1963, 85: 519−527.
[29] KULLMER G, RICHARD H A. Influence of the root radius of crack-like notches on the fracture load of brittle components [J]. Archive of Applied Mechanics, 2006, 76(11−12): 711−723.
[30] IOAKIMIDIS N I. Application of quantifier elimination to mixed-mode fracture criteria in crack problems [J]. Archive of Applied Mechanics, 2017, 87(10): 1567−1604.
[31] CHANG K J. On the maximum strain criterion-a new approach to the angled crack problem [J]. Engineering Fracture Mechanics, 1981, 14(1): 107−124.
[32] PALANISWAMY K, KNAUSS W G. Propagation of a crack under general in-plane tension [J]. International Journal of Fracture, 1972, 8(1): 114−117.
[33] SIH G C. Strain energy density factor applied to mixed mode crack problem [J]. International Journal of Fracture, 1974, 10(3): 305−321.
[34] YEHIA N A B. Distortional strain energy density criterion: The Y-criterion [J]. Engineering Fracture Mechanics, 1991, 39(3): 477−485.
[35] RAO Q H, SUN Z Q, STEPHANSSON O, LI C L, STILLBORG B. Shear fracture (Mode II) of brittle rock [J]. International Journal of Rock Mechanics and Mining Sciences, 2003, 40(3): 355−375.
[36] LI Peng, RAO Qiu-hua, LI Zhuo, JING Jing. Thermal-hydro-mechanical coupling stress intensity factor of brittle rock [J]. Transactions of Nonferrous Metals Society of China, 2014, 24(2): 499−508.
[37] LI Peng, RAO Qiu-hua, MA Wen-bo, SU Shu-lan, MA Chun-de. Coupled thermal-hydro-mechanical fractographic analysis of brittle rock [J]. Chinese Journal of Rock Mechanics and Engineering, 2014, 33(6): 1179−1186. (in Chinese)

脆性岩石热−水−力−化学(THMC)耦合裂纹扩展速率测试新方法

易 威，饶秋华，李 卓，沈晴晴

中南大学 土木工程学院，长沙 410075

摘 要：提出连续测量脆性岩石热−水−力−化学(THMC)耦合裂纹扩展速率的新型导电碳膜电测法。利用自行设计的耦合加载系统，连续测量不同温度下预制红砂岩试件 THMC 耦合裂纹扩展速率。结果表明：随着温度的增加，红砂岩试件起裂时间缩短，裂纹扩展速率和加速度增大。通过能量法计算的理论结果与试验结果吻合较好，验证 THMC 耦合裂纹扩展速率导电碳膜电测法的有效性。该方法能克服传统电法不能连续测量裂纹扩展速率以及光学法和声法不能测量多场耦合裂纹扩展速率的缺点，为 THMC 耦合作用下深部岩体工程的安全评估和止裂设计提供重要的理论依据。

关键词：裂纹扩展速率；导电碳膜电测法；热−水−力−化学耦合；能量法；脆性岩石

(Edited by Bing YANG)